Progress In Electromagnetics Research, Vol. 117, 283–298, 2011

PERIODIC TIME-VARYING NOISE IN CURRENT-COMMUTATING CMOS MIXERS

B. Guo* **and G. Wen**

School of Communication and Information Engineering, University of Electronic Science and Technology of China, Chengdu, China

Abstract—An analytical approach based on linear periodic time-varying theory, is developed to analyze the noise characteristics of current-commutating CMOS mixers. Based on the derived transfer functions with memory effect of tail capacitance, the frequency-dependent noise transforming factors for individual stages in the mixers are numerically computed to rigorously describe the noise output. A unified noise expression considering both the thermal noise and the flicker noise is proposed. It enables the noise analysis of the mixers particularly for a high LO frequency with different IF characteristics, and is verified by measurements.

1. INTRODUCTION

Direct conversion receivers (DCR) with the advantage of low cost and high integration, have gained more increased commercial market quotient among various receiver architectures [9]. For DCR, not only thermal noise from mixers, but also flicker noise can seriously deteriorate the overall system performance. On the other hand, the active mixer in which switching pairs are used for current commutating is more attractive in many applications because it provides higher conversion gain, resulting in improved suppression of noise contribution from subsequent stages [1, 10]. Therefore it is undoubtedly significant to accurately analyze and predict the noise characteristics of current-commutating mixers [2].

Different from the time invariant noise in low noise amplifiers [3], the time varying characteristic of noise in mixers complicates its analysis process much [11]. Until now, efforts to understand noise in mixers on a more intuitive basis only have resulted in a few

Received 7 April 2011, Accepted 3 June 2011, Scheduled 10 June 2011
* Corresponding author: Benqing Guo (benqingguo@hotmail.com).

representative analytical methods [4, 5]. The physical analytical model proposed in [5] roughly approximates that switching pairs commutate instantly, and resulting periodic noise pulses are randomly modulated by the ideal rectangular output current, which is only appropriate for a large sinusoidal LO swing. As the memory elements such as capacitors are commonly ignored, these approaches are only valid for low frequency, which thus makes the practical design of mixers with high LO frequency greatly dependent on the CAD tools such as Cadence, ADS and etc. In this work, an analytical approach based on linear periodic time-varying (LPTV) theory, is developed to analyze the noise characteristics of the mixer, incorporating memory effect of tail capacitance. The proposed analysis approach is a generalization for [4], and ultimately validated by measurements.

The paper is organized as follows. In Section 2, the noise analysis for the mixer is presented through deriving corresponding periodic transfer functions. And in Section 3, measurements verify the theory. Finally, conclusions are drawn in Section 4.

2. NOISE ANALYSIS

Without losing generality, the current-commutating CMOS mixer shown in Fig. 1 is examined. It is composed of an input transconductance stage (M_3), switching pairs (M_1 and M_2), and output loads (R_L). In principle, M_1 and M_2 commutate the tail current I_3 under the control of LO signal $V_{LO}(t)$ and complete the frequency transformation from the RF to the IF, while M_3 converts the RF voltage signal v_{RF} to the current i_{RF}. In GHz frequency range, parasitic effects can not be neglected. Tail capacitance observed towards x is generally far more than other nets and becomes a main bottleneck limiting noise performance in high frequency [4]. On the other hand, this capacitance consists of the gate-source capacitance of M_1 and M_2 (i.e., C_{gs1} and C_{gs2}) and the junction capacitances at the source of M_1 and M_2 and the drain of M_3. Since they appear as a nonlinear function of the applied voltage, these junction capacitances make the following analysis using the linear periodic time-varying theory exceedingly complicated. To overcome this difficulty, we approximate these junction capacitances as a time-invariant capacitance C_{eff}. As a result, the total capacitance at the tail node is the sum of C_{gs1}, C_{gs2} and C_{eff} just as in [5], and is defined as a time-invariant C_p illustrated by the dash line in Fig. 1.

The noise is contributed by all the devices in theory. Based on the derived transfer functions with the tail capacitance C_p, the frequency-dependent noise characteristic in the mixer, is systematically analyzed

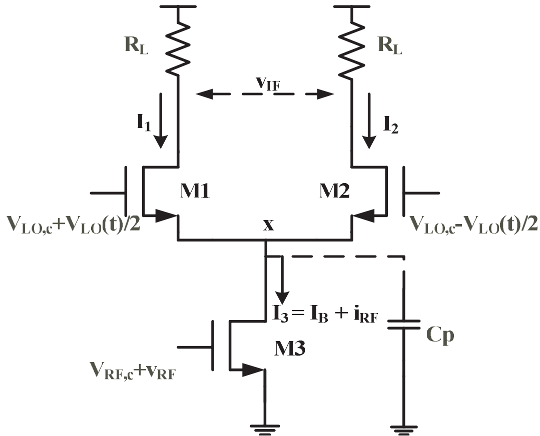

Figure 1. Current-commutating CMOS mixer.

using LPTV theory throughout this section. For clarity of discussion, the review of the fundamental LPTV theory is also summarized in the appendix [6].

2.1. Noise from the Transconductance Stage

By small signal analysis, the fundamental transfer function from the RF port to the IF port, takes the form

$$P\left(t,\omega\right)=\frac{g_{m1}-g_{m2}}{g_{m1}+g_{m2}+j\omega C_{p}} \tag{1}$$

where parameter $g_{m1,2}$ is transconductance of $M_{1,2}$, and can be iteratively solved by switching pairs' equation in [4]. $P(t,\omega)$ is periodic since $g_{m1,2}$ is time-varying in one LO period, T_{LO}. According to the appendix, we thus can derive nth order frequency-dependent Fourier coefficient of $P(t,\omega)$ as below

$$P_{n}\left(\omega\right)=\frac{1}{T_{LO}}\int_{0}^{T_{LO}}P\left(t,\omega-n\omega_{LO}\right)\exp\left(-jn\omega_{LO}t\right)dt \tag{2}$$

where ω_{LO} donates the LO angular frequency.

As a result, the conversion gain (CG) of the current-commutating mixer is

$$CG=c\left(\omega\right)\cdot g_{m3}R_{L} \tag{3}$$

where parameters $c(\omega)$ and g_{m3} are the switching pairs gain coefficient and transconductance for M_3. According to (A5), for the down conversion action with RF frequency f_{RF} being higher than LO frequency f_{LO} we can have

$$c\left(\omega_{IF}\right)=\left|P_{-1}\left(\omega_{IF}\right)\right|=\left|\frac{1}{T_{LO}}\int_0^{T_{LO}}\frac{g_{m1}-g_{m2}}{g_{m1}+g_{m2}+j\omega_{RF}C_p}\exp\left(j\omega_{LO}t\right)dt\right| \tag{4}$$

where ω_{RF} and ω_{IF} are the RF and IF angular frequency, and ω_{RF} corresponds to $\omega_{LO}+\omega_{IF}$. When f_{LO} is high enough (here we take IF frequency f_{IF} near to zero for convenience of expressing and exemplifying in Fig. 2. As for higher f_{IF}, things are similar only with further decreased amplitude), RF signal will be inevitably attenuated by the parasitic C_p. In other words, as shown in Fig. 2, the transfer function $p(t,\omega)$ is lowered, and the waveform amplitude of that is even less than one. So $c(\omega)$ is decreased correspondingly. Fig. 3 displays the relation of $c(\omega)$ vs. the bias current I_B with different f_{LO}.

In transconductance stage, the noise sources include the thermal channel noise current of M_3, the input source resistance R_s and the polysilicon gate resistance r_{g3}. According to the LPTV theory, the noise power spectral density (PSD) transformed to the output due to the wide-sense-stationary (WSS) noise input at the transconductance stage is

$$S_{n3}^{o}\left(\omega\right)=\sum_{n=-\infty}^{\infty}\left|P_n\left(\omega\right)\right|^2\cdot 4kT\left(R_s+r_{g3}+\frac{\gamma}{g_{m3}}\right)g_{m3}^2 \tag{5}$$

where γ is the noise coefficient of devices. And we also define the noise transforming factor of transconductance stage $\alpha\left(\omega\right)=\sum\limits_{n=-\infty}^{\infty}\left|P_n\left(\omega\right)\right|^2$.

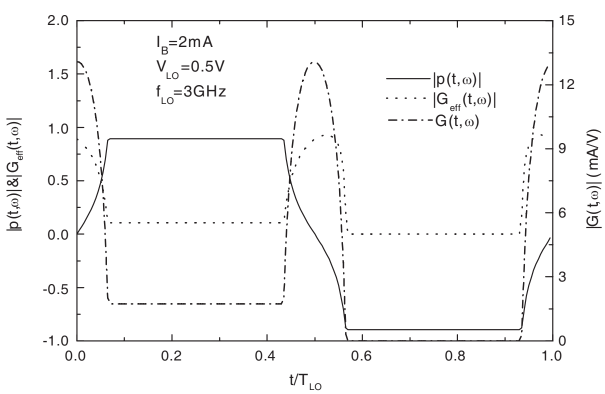

Figure 2. $|P(t,\omega)|$, $|G_{eff}(t,\omega)|$, and $|G(t,\omega)|$ in T_{LO} when $I_B=2\,\mathrm{mA}$, $V_{LO}=0.5\,\mathrm{V}$, $f_{LO}=3\,\mathrm{GHz}$.

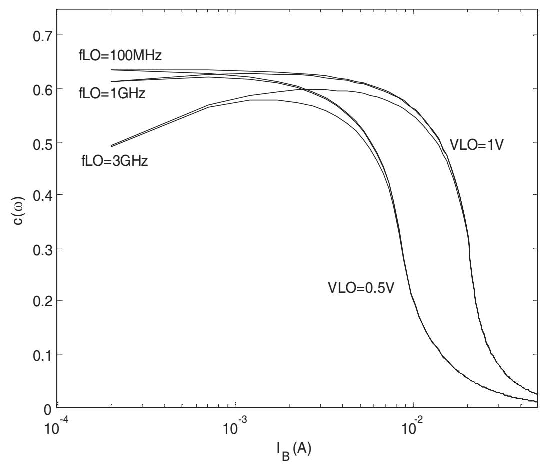

Figure 3. Numerically computed gain coefficient $c(\omega)$.

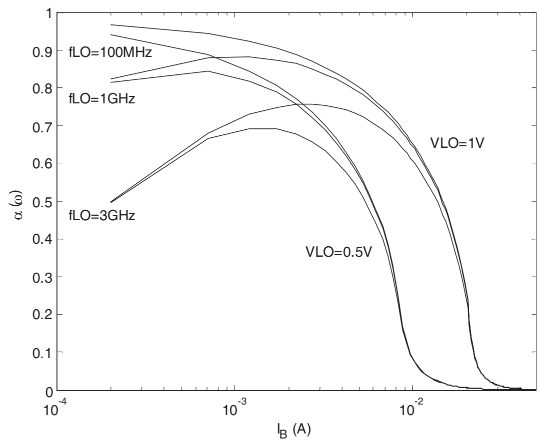

Figure 4. Numerically computed transforming factor $\alpha(\omega)$.

As shown in Fig. 4, high f_{LO} will decrease the numerical value of $\alpha(\omega)$, which is similar to $c(\omega)$.

2.2. Noise from the LO Port Resistance

Similarly, the periodic transfer function from the LO port at the gate of M_1 and M_2 side, respectively to the differential IF port, $G(t,\omega)$ and

$H(t,\omega)$ take the form as below

$$G(t,\omega)=\frac{g_{m1}\left(2g_{m2}+j\omega C_p\right)}{g_{m1}+g_{m2}+j\omega C_p}\quad H(t,\omega)=\frac{g_{m2}\left(2g_{m1}+j\omega C_p\right)}{g_{m1}+g_{m2}+j\omega C_p}. \tag{6}$$

Due to the periodicity of switching pairs functioning one can see $g_{m1}(t)=g_{m2}(t-T_{LO}/2)$ and $g_{m2}(t)=g_{m1}(t-T_{LO}/2)$. Meanwhile, according to LPTV theory, we can have the below relationship of nth order frequency-dependent Fourier coefficient $G_n(\omega)$ and $H_n(\omega)$

$$\begin{aligned} G_n(\omega)=&\frac{1}{T_{LO}}\int_0^{T_{LO}} G(t,\omega-n\omega_{LO})\exp(-jn\omega_{LO}t)\,dt\\ H_n(\omega)=&\frac{1}{T_{LO}}\int_0^{T_{LO}} H(t,\omega-n\omega_{LO})\exp(-jn\omega_{LO}t)\,dt\\ =&\frac{1}{T_{LO}}\int_0^{T_{LO}} G(t-T_{LO}/2,\omega-n\omega_{LO})\exp(-jn\omega_{LO}t)\,dt\\ =&G_n(\omega)/(-1)^n \end{aligned} \tag{7}$$

Considering the symmetry of switching pairs, the noise contribution to the output at LO port thus is simplified as

$$\begin{aligned} S_{nLO}^{o}(\omega) &= \sum_{n=-\infty}^{\infty}|G_n(\omega)|^2 4kT(R_{LO}/2+r_{g1})\\ &\quad+\sum_{n=-\infty}^{\infty}|H_n(\omega)|^2 4kT(R_{LO}/2+r_{g2})\\ &= \sum_{n=-\infty}^{\infty}|G_n(\omega)|^2 4kT(R_{LO}+2r_{g1}) \end{aligned} \tag{8}$$

where R_{LO}, $r_{g1,2}$ are the equivalent noise resistance of LO port, and the polysilicon gate resistance of $M_{1,2}$. And we also define the noise transforming factor of switching pairs $\beta(\omega)=\sum\limits_{n=-\infty}^{\infty}|G_n(\omega)|^2$.

The periodic waveform in T_{LO} for the transfer function $|G(t,\omega)|$ is also exemplified in Fig. 2 with the typical $I_B=2\,\text{mA}$, $V_{LO}=0.5\,\text{V}$, and $f_{LO}=3\,\text{GHz}$. Fig. 5 depicts the relation of $\beta(\omega)$ vs. I_B with different f_{LO}.

2.3. Noise from Switching Transistors

Since the channel noise of switching transistors is cyclostationary instead of WSS, the related analysis gets troublesome. Fortunately, the cyclostationary noise source can be modeled as modulated stationary

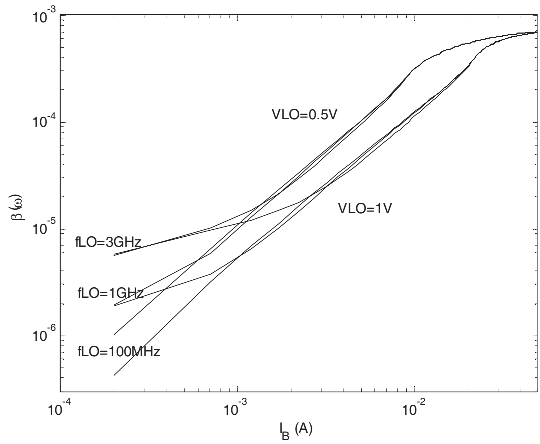

Figure 5. Numerically computed transforming factor of LO port at M_1 side $\beta(\omega)$.

noise sources. And the modulated effect can be incorporated in the periodic transfer function. Take M_1 for example, its cyclostationary noise $4\,\mathrm{kT}\gamma g_{m1}$ is modeled as a WSS noise $4\,\mathrm{kT}\gamma g_{m1\max}$ modulated by a periodic waveform with normalized amplitude $g_{m1}/g_{m1\max}$ ($g_{m1\max}$ being the maximum of g_{m1} in T_{LO}). The corresponding effective periodic transfer function with modulated effect, thus takes the form

$$G_{\mathit{eff}}\,(t,\omega)=\sqrt{\frac{g_{m1}}{g_{m1,\max}}}\frac{2g_{m2}+j\omega C_p}{g_{m1}+g_{m2}+j\omega C_p}. \tag{9}$$

And we also define the effective noise transforming factor of switching pairs $\beta_{\mathit{eff}}\,(\omega)=\sum\limits_{n=-\infty}^{\infty}|G_{\mathit{eff},n}\,(\omega)|^2$. Then we also have

$$G_{\mathit{eff},n}\,(\omega)=\frac{1}{T_{LO}}\int_0^{T_{LO}}G_{\mathit{eff}}\,(t,\omega-n\omega_{LO})\exp\left(-jn\omega_{LO}t\right)dt. \tag{10}$$

As a result, the noise PSD contribution to the output due to M_1 is

$$S^o_{n1,wte}\,(\omega)=\sum_{n=-\infty}^{\infty}|G_{\mathit{eff},n}\,(\omega)|^2 4KT\gamma\cdot g_{m1,\max}. \tag{11}$$

The periodic waveform of transfer function $|G_{\mathit{eff}}(t,\omega)|$ in T_{LO} is also quantitatively depicted in Fig. 2 with the same $I_B=2\,\mathrm{mA}$, $V_{LO}=0.5\,\mathrm{V}$, and $f_{LO}=3\,\mathrm{GHz}$. As shown in Fig. 6, high f_{LO} will roughly increase the numerical value of effective noise transforming factor of switching pairs $\beta_{\mathit{eff}}(\omega)$, which is similar to $\beta(\omega)$.

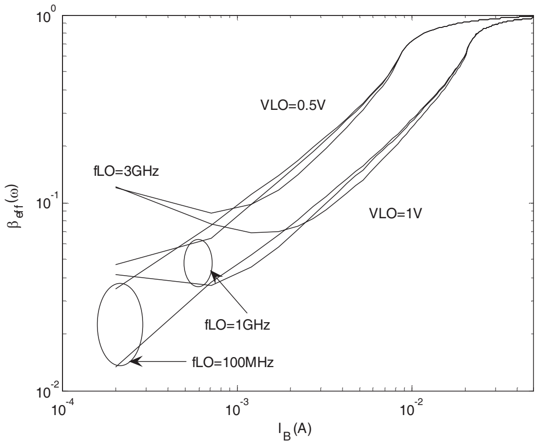

Figure 6. Numerically computed effective transforming factor $\beta_{\mathit{eff}}(\omega)$.

2.4. Flicker Noise

The flicker noise of the mixer exclusively arises from the leakage from switching pairs $M_{1,2}$ [4, 5]. Considering the characteristic of flicker noise, its output PSD due to M_1 can be simplified from (8) as follows

$$S^o_{n1,flk}(\omega) = |G_0(\omega)|^2 \overline{V^2_{n1}}. \tag{12}$$

where parameter $G_0(\omega)$ is the time-average of transfer function $G(t, \omega)$ in T_{LO}, and can be obtained according to (7). Moreover, the flicker noise of M_1 is [5]

$$\overline{V^2_{n1}} = \frac{K_f}{C_{OX} W_1 L} \frac{1}{f} \tag{13}$$

where parameter K_f is a process parameter. This model is not as accurate as the BSIM3v3 model, but serves as analytical formulation and has been extensively used to model flicker noise for the first-order approximate solutions.

2.5. Noise Figure

Based on the noise contributions in above, with the symmetry of switching pairs, the single sideband (SSB) noise figure (NF) for the current-commutating mixer is

$$NF = \frac{S^o_{n3}(\omega) + 2S^o_{n1,wte}(\omega) + 2S^o_{n1,flk}(\omega) + S^o_{nLO}(\omega) + S^o_{nRL}}{c(\omega)^2 g^2_{m3} 4kTR_s} \tag{14}$$

where the noise from the loads R_L, S_{nRL} is

$$S^o_{nRL} = 8kT/R_L. \tag{15}$$

On the whole, this noise expression is unified in that it consists of not only the thermal noise but also the flicker noise, which thus make it suitable for the current-commutating mixer with different IF characteristics. If f_{IF} is high enough to make the flicker noise close to zero and C_p is neglected, (14) reduces to the conventional prediction expression for low frequency in [4]. As shown in the next section, only by numerically computing several frequency-dependent noise transforming factors, the noise characteristic of the mixer can be conveniently predicted even if f_{LO} is high, which is fairly desirable for designs and optimizations.

3. RESULTS AND DISCUSSIONS

To validate the analysis experimentally, the SSB noise figures of a current-commutating mixer fabricated in Chartered 0.18 µm CMOS technology were measured at low and high point frequencies, respectively. Low and high point frequencies of 100 kHz and 100 MHz were obtained by tuning the frequency of RF input signal while the LO frequencies were fixed at 1 GHz and 3 GHz, respectively. The measurement setup and micrograph of die are shown in Fig. 7, where an off-chip balun was used to generate the differential LO signal for

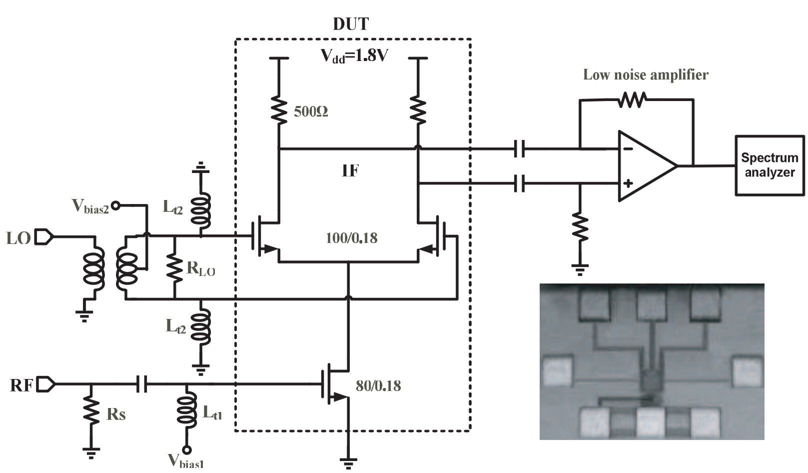

Figure 7. Measurement setup of current-commutating CMOS mixer and die micrograph.

Table 1. Summary of extracted parameters for simulations.

K_1	$77.8\,\mathrm{mA/V^2}$	r_{g3}	$8.26\,\Omega$
θ	2.76	$r_{g1,2}$	$10.33\,\Omega$
R_s	$50\,\Omega$	C_p	310 fF
R_{LO}	$50\,\Omega$	K_f	8.5E-24V^{2}F

switched pairs. Off-chip inductors L_{t1}, L_{t2} were tuned at RF and LO frequency to absorb the net parasitic capacitances at RF port and LO port, and provided the corresponding impendence matching. V_{bias1} and V_{bias2} are DC biases of RF port and LO port, respectively. To measure the output noise, a low noise amplifier (using LT1007) was adopted to convert differential current noise into single-ended one and feed it to the spectrum analyzer. The noise contribution from this active balun acted as the test load, has been deducted from the test data. The extracted parameters for numerical simulations are shown in Table 1 where parameters K_1 and θ obey the definition in [4]. Especially, the noise coefficient for short channel devices γ approximately takes 2.5 [7].

The expression (14) is a unified expression for estimating the noise of the mixer with different IF characteristics. According to the IF being high or low, the analysis is discussed as follows, respectively.

In superheterodyne receiver with high IF, flicker noise is negligible. Take $f_{IF} = 100\,\mathrm{MHz}$ for example, the noise and gain characteristic is compared between predictions and measurements. As shown in Fig. 8, the optimum NF appears at lower current than the optimum CG does. Take $V_{LO} = 0.5\,\mathrm{V}$, $f_{LO} = 1\,\mathrm{GHz}$ for example, the simulated optimum NF is 11.7 dB at $I_B = 1.5\,\mathrm{mA}$ while the simulated optimum CG is 13.2 dB at $I_B = 3.8\,\mathrm{mA}$. In view of power consumption, it is desirable that I_B takes 1.5 mA, since the signal noise ratio is little changed in this current range. Similarly it is also true to the analysis for $V_{LO} = 0.5\,\mathrm{V}$, $f_{LO} = 3\,\mathrm{GHz}$ although the corresponding optimum NF and CG is increased by 0.5 dB and -0.3 dB or so, respectively. The reason for this is attributed to the deteriorated transforming factors $c(\omega)$, $\alpha(\omega)$, $\beta(\omega)$, and $\beta_{\mathit{eff}}(\omega)$ resulted by increased f_{LO} as in Figs. 3–6.

For the DCR with low IF, flicker noise will get prominent. Fig. 9 presents the measured mixer output current noise PSD with $f_{LO} = 3\,\mathrm{GHz}$, where the bias I_B is fixed at 1 mA and V_{LO} takes 0.5 and 1 V, respectively. The frequency (i.e., f_{IF}) is scanned between 10 kHz and 500 kHz. As in the figure, the spectrum of measured noise clearly exhibits a $1/f$ frequency dependency. And higher V_{LO} notably reduces the flicker noise output, which is consistent with the results observed in [4].

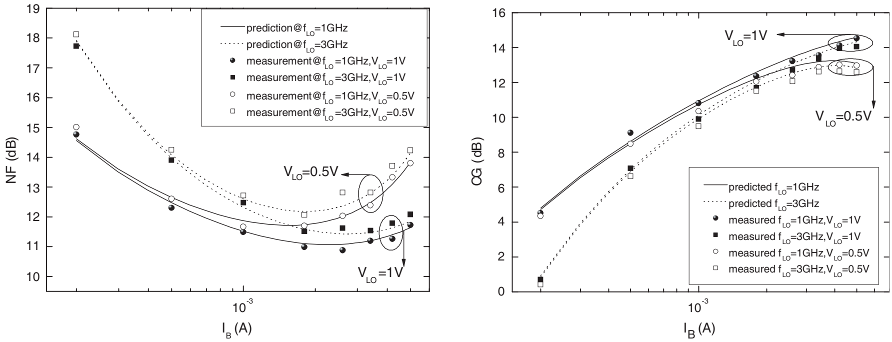

Figure 8. Predicted and measured NF and CG vs. I_B at f_{IF} = 100 MHz.

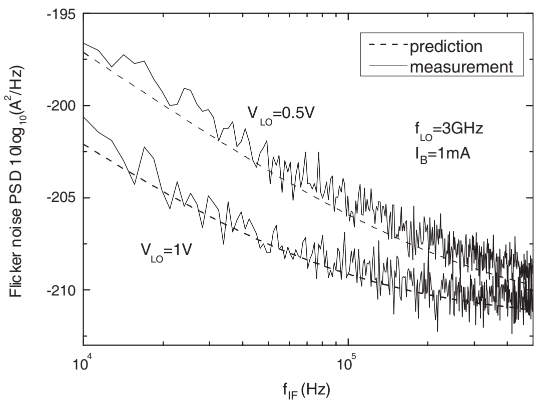

Figure 9. Predicted and measured flicker noise PSD of the mixer.

Then take the fixed $f_{IF} = 100\,\text{kHz}$ for example, the noise characteristic is examined with the typical $V_{LO} = 0.5, 1\,\text{V}$ and $f_{LO} = 1, 3\,\text{GHz}$, respectively. As shown in Fig. 10, it is noted that the optimum NF appears at lower current than that for high IF case in Fig. 8. Take $V_{LO} = 1\,\text{V}$ for example, the simulated optimum NF is about 1339 dB at $I_B = 0.6\,\text{mA}$ for $f_{LO} = 1\,\text{GHz}$ while it takes 1518 dB or so at $I_B = 1\,\text{mA}$ for $f_{LO} = 3\,\text{GHz}$. The reason for this phenomenon lies in that the NF for low IF is clearly increased due to the flicker noise from switching pairs.

According to (4), the conversion gain for low f_{IF} in principle should be higher than that for high f_{IF} because for low f_{IF}, a lower RF signal in equivalence is applied to the gate of M3 under the fixed f_{LO}. However, f_{LO} is normally far higher than f_{IF} (no matter low and high f_{IF}), which makes CG differences due to the different f_{IF} quite subtle,

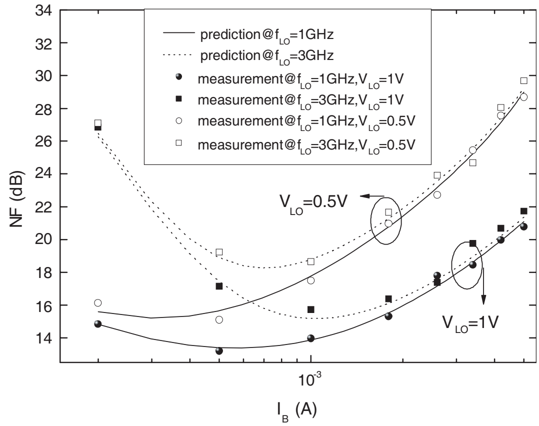

Figure 10. Predicted and measured NF vs. I_B at $f_{IF} = 100\,\text{kHz}$.

and normally comparable to measurement errors On the other hand, if f_{IF} is fixed, a high f_{LO} leads to a clearly low conversion gain since the absolute variation of f_{LO} is much larger than the f_{IF} itself. Here, take $V_{LO} = 1\,\text{V}$ for example, with the fixed $f_{IF} = 100\,\text{MHz}$ and $I_B = 1\,\text{mA}$, the simulated CG shown in Fig. 8 is 10.97 dB for $f_{LO} = 1\,\text{GHz}$, but decreases to 10.14 dB for $f_{LO} = 3\,\text{GHz}$. The CG results for low f_{IF} case are little different from high f_{IF} case in Fig. 8, and therefore are omitted.

From above analysis, (14) and (3) can assist designers to obtain the improved noise and conversion gain performances by capturing the optimized bias current under different LO levels. As the parasitic tail capacitance is considered, the two predicted expressions make them effectively applicable to high f_{LO} situations On the whole, for both IF characteristics, the measured NF and CG well agree with the predictions even when f_{LO} becomes as high as 3 GHz. Additionally, Cadence simulations also justify our theory's validity below 5 GHz The proposed approach based on LPTV theory also is of possibility to predict noise at even higher frequency provided that more net capacitances in the mixer are included in the transfer functions, although which often makes the related derivations too complex in effect to gain intuitive insights (For example, gain drain capacitances C_{gd} of $M_{1,2}$ are not included in our analysis in the interest of simplicity). The NF discrepancy between predictions and measurements is mainly attributed to the fact that parameter γ is not solely dependent on channel length of devices, but related to bias current, drain and body voltage of devices. For example, a recent research finds that low current density generally yields a small γ [8].

4. CONCLUSIONS

An analytical approach based on linear periodic time-varying theory is developed to analyze the noise characteristics of current-commutating CMOS mixers. Based on the derived transfer functions with memory effect of tail capacitance, the frequency-dependent noise transforming factors for individual stages in the mixers are numerically computed to rigorously describe the noise output. A unified noise figure expression including both the thermal noise and the flicker noise has been proposed. It displays advantages particularly when LO frequency is high, and therefore can serve as a guideline for predicting and optimizing noise of the mixers in different receiver architectures.

ACKNOWLEDGMENT

This work was funded by Natural Science Foundation of China (Grant No. 60688101). The authors would like to thank Prof. Jianguo Ma in Tianjin University for the guidance and support.

APPENDIX A.

The relation between the input $x(t)$ and the output $y(t)$ for a linear time-varying system, can be given by

$$y(t) = \int_{-\infty}^{\infty} h(t,u)\, x(u)\, du = \frac{1}{2\pi}\int_{-\infty}^{\infty} H(t,\omega)\, X(\omega)\, e^{j\omega t} dt \qquad \text{(A1)}$$

where $h(t,u)$ is the impulse response with u denoting the launch time and t denoting the observation time, and $H(t,\omega)$ is the time-varying transfer function with ω donating the angular frequency corresponding to the delay ν $(= t-u)$. Moreover, $h(t,u)$ and $H(t,\omega)$ are a pair of Fourier transform with respect to ν,

$$\begin{aligned} h(t,u) &= \frac{1}{2\pi}\int_{-\infty}^{\infty} H(t,\omega)\, e^{j\omega v} d\omega \\ H(t,\omega) &= \int_{-\infty}^{\infty} h(t,u)\, e^{-j\omega v} dv. \end{aligned} \qquad \text{(A2)}$$

Mixers driven by the periodic LO signal are commonly modeled as LPTV systems [2, 7]. As a result, $h(t,u)$ and $H(t,\omega)$ for mixers become periodic with respect to T_{LO}, and can be represented by Fourier series (assumed to converge), i.e., [6]

$$h(t,u) = \sum_{n=-\infty}^{\infty} h_n(v)\, e^{jn\omega_{LO} u}$$

$$H(t,\omega) \;=\; \sum_{n=-\infty}^{\infty} H_n(\omega + n\omega_{LO})\, e^{jn\omega_{LO}t} \tag{A3}$$

where $h_n(\nu)$ and $H_n(\omega)$ are nth order harmonic impulse response and nth order harmonic transfer function, respectively. We also can rewrite the bottom of (A3) in the form below

$$H_n(\omega) = \frac{1}{T_{LO}} \int_0^{T_{LO}} H(t, \omega - n\omega_{LO}) \exp(-jn\omega_{LO}t)\, dt. \tag{A4}$$

Substituting the top of (A3) into (A1) and taking Fourier transform to the resulting $y(t)$, we obtain

$$Y(\omega) = \sum_{n=-\infty}^{\infty} H_n(\omega)\, X(\omega - n\omega_{LO}) \tag{A5}$$

where $X(\omega)$ is the Fourier transform of deterministic input $x(t)$. Equations (A4) and (A5) well describe the frequency translation of mixers. Take down conversion for example, variables X, Y just correspond to RF input and IF output signal, respectively. Meanwhile, 1st harmonic coefficient is usually adopted for high conversion efficiency in mixers. Thus (A5) reduces to $Y(\omega_{IF}) = H_{-1}(\omega_{IF})X(\omega_{IF} + \omega_{LO})$ with n taking -1, representing f_{RF} located at the right sideband of f_{LO}. And the left sideband scenario can be described by taking $n = 1$. According to (A4), we can capture $H_{-1}(\omega_{IF})$ from $H(t, \omega_{IF} + \omega_{LO})$ derived from RF input to IF output in small signal circuit analysis. The conversion gain thus can be computed.

On the other hand, for a WSS noise input $x(t)$, the output $y(t)$ can be shown to be a cyclostationary process. Similarly, the autocorrelation function $R_y(t,\tau)$ and the output PSD $S_y(t,\omega)$ are also periodic with respect to T_{LO}, thus can be represented by Fourier series (assumed to converge), i.e., [6]

$$\begin{aligned} R_y(t,\tau) &= \sum_k R_y^k(\tau)\, e^{jk\omega_{LO}t} \\ S_y(t,\omega) &= \sum_k S_y^k(\omega)\, e^{jk\omega_{LO}t}. \end{aligned} \tag{A6}$$

And we have the definition of the output autocorrelation harmonic function [6]

$$R_y^k(\tau) = \lim_{T_{LO}\to\infty} \frac{1}{T_{LO}} \int_{-T_{LO}/2}^{T_{LO}/2} R_y\left(t + \frac{\tau}{2}, t - \frac{\tau}{2}\right) e^{-jk\omega_{LO}t} dt \tag{A7}$$

where τ is the correlation time. Furthermore, the output autocorrelation harmonic function $R_y^k(\tau)$ and the output PSD harmonic function $S_y^k(\omega)$ constitute another pair of Fourier transform. As a result, the output autocorrelation harmonic function of mixers is obtained by substituting (A1) and (A3) into (A7)

$$R_y^k(\tau) = \sum_{n=-\infty}^{\infty} \left[\langle R_x(\tau) \rangle e^{-j\frac{\pi}{T_{LO}}(2n-k)\tau} \right] \otimes r_{n,(n-k)}^k(-\tau) \tag{A8}$$

where

$$r_{n,(n-k)}^k(\tau) = \int_{-\infty}^{\infty} h_n\left(t+\frac{\tau}{2}\right) h_{n-k}^*\left(t-\frac{\tau}{2}\right) e^{-jk\omega_{LO}t} dt.$$

Here, symbols "$\otimes$" and "$*$" indicate convolution and conjugate operation, respectively. Moreover, the definition of autocorrelation function for WSS noise input $x(t)$ is [6]

$$\langle R_x(\tau) \rangle = \lim_{T_{LO}\to\infty} \frac{1}{T_{LO}} \int_{-T_{LO}/2}^{T_{LO}/2} R_x\left(t+\frac{\tau}{2}, t-\frac{\tau}{2}\right) dt. \tag{A9}$$

Taking Fourier transform to (A8) yields

$$\begin{aligned} S_y^k(\omega) \;=\; & \sum_{m=-\infty}^{\infty} H_{m+k}\left(\omega+\frac{k\omega_{LO}}{2}\right) \left\langle S_x\left(\omega-\left(\frac{k}{2}+m\right)\omega_{LO}\right)\right\rangle \\ & H_m^*\left(\omega-\frac{k\omega_{LO}}{2}\right). \end{aligned} \tag{A10}$$

According to LPTV theory, the PSD of the cyclostationary process at any two frequencies that are separated by multiples of the LO frequency are correlated. The correlations in different components of $S_y^k(\omega)$ may constitute potential problems in mixers. Fortunately, after limited bandwidth filtering with central frequency ω, the components of $S_y^k(\omega)$ for $k \neq 0$ are eliminated. As a result, the output of mixers becomes stationary and the resulting output spectrum simply is the time average of $S_y(t,\omega)$ in T_{LO} as shown below

$$S_y^0(\omega) = \overline{S_y(t,\omega)} = \sum_{n=-\infty}^{\infty} |H_n(\omega)|^2 S_x(\omega - n\omega_{LO}). \tag{A11}$$

If mixers are memoryless, we have $h(t,u) = h(t)\delta(t-u)$ and therefore $y(t) = h(t)x(t)$. Substituting it into (A2) and (A3), we have $H(t,\omega) = h(t)$ and $H_n(\omega) = H_n$. Its PSD thus reduces to $S_y(\omega) = \sum\limits_{n=-\infty}^{\infty} |H_n|^2 S_x(\omega - n\omega_{LO})$, which is simply assumed in the conventional analysis for mixers.

REFERENCES

1. Wei, H.-C., R.-M. Weng, and S.-Y. Li, "A broadband high linearity and isolation down-conversion mixer for WiMAX applications," *Journal of Electromagnetic Waves and Applications*, Vol. 23, No. 11–12, 1555–1565, 2009
2. Hull, C. D. and R. G. Meyer, "A systematic approach to the analysis of noise in mixers," *IEEE Trans. Circuits Syst. I*, Vol. 40, 909–919, 1993.
3. Yoon, J., H. Seo, I. Choi, and B. Kim, "Wideband LNA using a negative gm cell for improvement of linearity and noise figure," *Journal of Electromagnetic Waves and Applications*, Vol. 24, No. 5–6, 619–630, 2010.
4. Terrovitis, M. T. and R. G. Meyer, "Noise in current-commutating CMOS mixers," *IEEE J. Solid-State Circuits*, Vol. 34, 772–783, 1999.
5. Darabi, H. and A. A. Abidi, "Noise in RF-CMOS mixers: A simple physical model," *IEEE J. Solid-State Circuits*, Vol. 35, 15–25, 2000.
6. Gardner, W. A., *Introduction to Random Processes with Applications to Signals and Systems*, 2nd edition, McGraw-Hill, New York, 1989.
7. Lee, T. H., *The Design of CMOS Radio-Frequency Integrated Circuits*, 2nd edition, Cambridge University Press, New York, 2004.
8. Li, Z. and J. Ma, "Compact channel noise models for deep-submicron mosfet," *IEEE Trans. Electron Devices*, Vol. 56, 1300–1307, 2009.
9. De la Morena-Álvarez-Palencia, C. and M. Burgos-Garcia, "Four-octave six-port receiver and its calibration for broadband communications and software defined radios," *Progress In Electromagnetics Research*, Vol. 116, 1–21, 2011.
10. Guo, J., Z. Xu, C. Qian, and W.-B. Dou, "Design of a microstrip balanced mixer for satellite communication," *Progress In Electromagnetics Research*, Vol. 115, 289–301, 2011.
11. Park, C., H. Seo, and B. Kim, "A noise optimized passive mixer for charge-domain sampling applications," *Journal of Electromagnetic Waves and Applications*, Vol. 23, No. 14–15, 1909–1917, 2009.